

# Control of Femtosecond Filamentation by Field-Free Revivals of Molecular Alignment<sup>1</sup>

Jian Wu<sup>a</sup>, Hua Cai<sup>a</sup>, Yan Peng<sup>a</sup>, Yuqi Tong<sup>a</sup>, Arnaud Couairon<sup>b</sup>, and Heping Zeng<sup>a,\*</sup>

<sup>a</sup> State Key Laboratory of Precision Spectroscopy, East China Normal University, Shanghai, 200062 China

<sup>b</sup> Centre de Physique Théorique, CNRS, École Polytechnique, F-91128 Palaiseau, France

e-mail: hpzeng@phy.ecnu.edu.cn

Received February 28, 2009

**Abstract**—We show that the filamentation dynamics of a femtosecond laser probe pulse can be readily controlled by properly matching it to the quantum revivals of pre-aligned molecules prepared through impulsive rotational Raman excitation with an advancing ultrashort pump pulse. Several features of the filamentation process including supercontinuum generation, the length of the plasma channel generated in the wake of the filament, the associated secondary radiations and the multiple filamentation pattern are all easily modified by tuning the cross phase modulation induced by the field-free revivals of molecular alignment, through the delay between the pump and the probe pulses. We show that molecular alignment can also be used to generate conical waves with extremely short intensity spike called shocked X-waves and to further tune the frequency of a few-cycle laser pulse in the wake of a self-guided intense filament.

PACS numbers: 42.65.Jx, 52.38.Hb, 37.10.Vz, 33.80.-b

DOI: 10.1134/S1054660X09150444

## 1. INTRODUCTION

Intense ultrashort laser pulses propagating in transparent nonlinear media typically undergo filamentation, which denotes a peculiar propagation regime with a well confined beam radius of  $\sim 50 \mu\text{m}$  and high peak-intensity of  $\sim 5 \times 10^{13} \text{ W/cm}^2$  over distances much longer than the Rayleigh length [1, 2]. It is now well established that several physical effects among which optical Kerr self-focusing, plasma defocusing, plasma and multiphoton absorptions as well as material diffraction/dispersion compete so as to maintain interaction of light with the medium over extended distances. In gases, many applications based on filaments are foreseen, such as light detection and ranging techniques [3], high-energy few-cycle laser pulse generation [4, 5], nonlinear frequency conversion [6], supercontinuum generation [7, 8], and THz emission [9]. Therefore, it is important to study practical methods to control the features of filaments with the aim of developing their potential applications. In contrast with atomic gases, molecular gases such as air can be prepared to orientate the diatomic molecules of  $\text{N}_2$  and  $\text{O}_2$  with respect to the field polarization of the pulse undergoing filamentation. Molecular alignment is known to exhibit periodic revivals several picoseconds after the impulsive rotational Raman excitation. This effect, known as the quantum wake, has been extensively studied for molecular orbital reconstruction [10], high harmonic generation [11], and recently for the propagation of ultrashort laser pulses [12–14]. In this paper, we show that the quantum wake consti-

tutes a versatile tool to control several important features of filamentation.

The main idea of the control mechanism is that a femtosecond pump pulse is used as impulsive rotational Raman excitation to align the molecules and a delayed femtosecond laser pulse which will undergo filamentation, hereafter called probe even if it is stronger than the pump, is then sent within the time window of the field-free revivals of the molecular alignment. By tuning the delay between both pulses, the probe will experience a cross phase modulation (XPM) effect which can be precisely tuned in space and time by matching the probe with the rising or falling edge of the quantum revivals. The filamentation process is strongly sensitive to XPM induced by the quantum revivals allowing us to readily control the dynamics of single- and multiple filamentation, the associated supercontinuum generation, the formation of conical optical shocks (shock X-wave), and to tune the frequency of few-cycle laser pulses in the quantum wake of a self-guided femtosecond filament.

## 2. IMPULSIVE MOLECULAR ALIGNMENT

For a molecular gas exposed to ultrashort laser pulses of duration much shorter than the corresponding rotational period, molecular alignment is not only achieved during the pulse duration but also exhibits periodic revivals after the extinction of the pump pulse [15]. This is due to the quantum beatings of the prepopulated rotational states  $|JM\rangle$ , where  $J = 0, 1, 2, \dots$  and  $M = -J, -J + 1, \dots, J - 1, J$  account for the orbital momentum and corresponding projection onto the

<sup>1</sup> The article is published in the original.

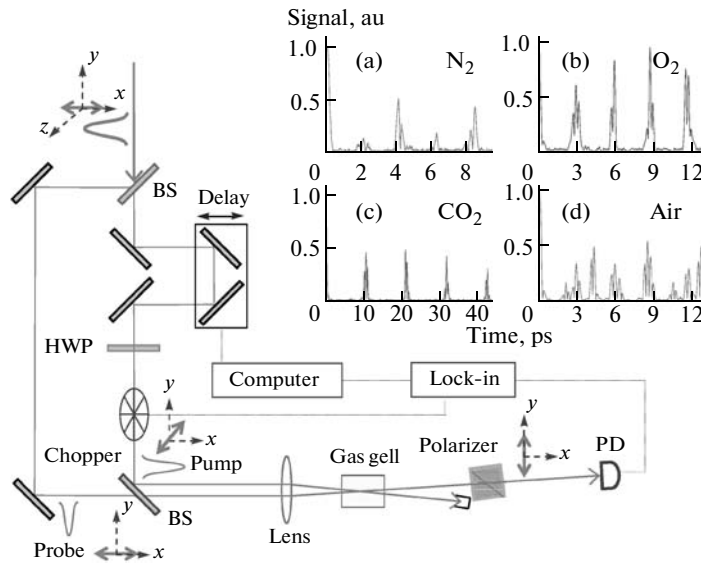


**Fig. 1.** Experimental setup used for measurements of molecular alignment by weak field polarization spectroscopy. BS: beam splitter; HWP: half-wave plate; PD: photodiode detector. The insets show the measured revivals of molecular alignment proportional to  $(\langle \cos^2 \theta \rangle - 1/3)^2$  for (a)  $N_2$ , (b)  $O_2$ , (c)  $CO_2$ , and (d) air.

symmetry axis of the molecule. In the case of an off-resonant excitation, the interaction of a linearly polarized pump pulse with linear molecules can be described by the effective Hamiltonian  $H = H_0 - 1/4\Delta\alpha E^2 \cos^2\theta$ , where  $H_0 = B_0J(J+1) + D_0J^2(J+1)^2$  denotes the field free Hamiltonian,  $\theta$  is the angle between the molecular axis and the field polarization of the pump pulse,  $B_0$  and  $D_0$  are the rovibrational molecular constants which determine the revival period,  $E(t)$  is the amplitude of the pump pulse, and  $\Delta\alpha = \alpha_{\parallel} - \alpha_{\perp}$  is the polarizability difference between the components parallel and perpendicular to the molecular axis. During the excitation by the pump pulse, the evolution of the molecular rotational state  $|\psi\rangle = \sum_{JM} C_{JM}|JM\rangle$  is calculated by integrating the Schrödinger equation  $i\hbar\partial|\psi\rangle/\partial t = H|\psi\rangle$ . After extinction of the pump, the population of each rotational state continues to evolve in the field-free Hamiltonian. The degree of molecular alignment is characterized by the quantity  $\langle \cos^2\theta \rangle$  which is calculated by a double averaging procedure: First the Schrödinger equation is solved for each initial molecular rotational state  $|\psi(t=0)\rangle = |J_0M_0\rangle$ , and the degree of molecular alignment at time  $t$  is obtained from the population  $C_{JM}(t)$  of each rotational state as:

$$\langle \cos^2\theta \rangle_{J_0M_0} = \sum_{JM, JM} C_{JM}^* C_{JM} \langle JM | \cos^2\theta | JM \rangle. \quad (1)$$

Then we considered that initial states are populated according to the temperature-dependent Boltzmann

distribution. The averaged degree of molecular alignment in the quantum wake is thus obtained by

$$\langle \langle \cos^2\theta \rangle \rangle = \frac{\sum_{J_0} P_{J_0} \sum_{M_0=-J_0}^{J_0} \langle \cos^2\theta \rangle_{J_0M_0}}{\sum_{J_0} P_{J_0}}, \quad (2)$$

where  $P_{J_0}$  is the population probability of state  $J_0$ . Its dependence upon temperature follows the Boltzmann distribution. For randomly oriented molecules, the average term  $\langle \cos^2\theta \rangle$  is equal to 1/3. The molecular orientation tends to be parallel to the field polarization when  $\langle \cos^2\theta \rangle$  is greater than 1/3, whereas smaller values indicate perpendicular orientation.

Experimentally, the molecular alignment was measured by weak field polarization spectroscopy [16] which is based on the modulation of the field polarization experienced by a probe pulse in oriented molecules. Our setup is shown in Fig. 1. By means of a half-wave plate, the polarization of the pump pulse was rotated by  $45^\circ$  with respect to the probe polarization. The modulations of the latter follow the revivals of the molecular alignment. A polarizer was used to transmit only the polarization component perpendicular to the incident polarization of the probe before measurement. The typical molecular alignment signal proportional to  $(\langle \cos^2\theta \rangle - 1/3)^2$  was measured by this conventional technique for linear molecules  $O_2$ ,  $N_2$ , and  $CO_2$  which exhibit revival periods of 11.6, 8.4, and 42.7 ps, respectively, as shown in the insets (a), (b), and (c) of Fig. 1. The hybrid molecular alignment sig-

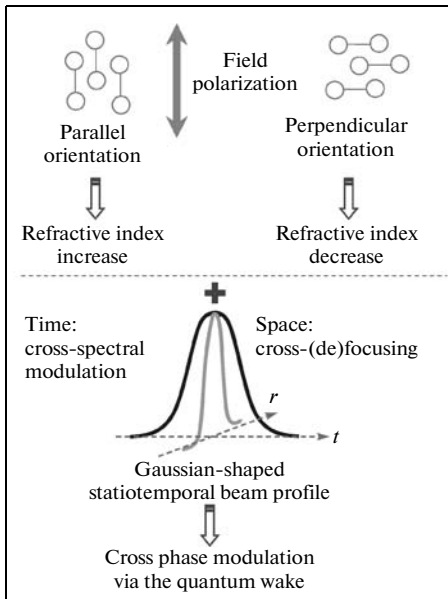


**Fig. 2.** Schematic representation of the cross phase modulation effect induced by the pump pulse with a Gaussian beam profile on a probe pulse via the revivals of molecular-alignment.

nal of air, composed of  $N_2$  and  $O_2$ , is also presented in the inset (d) of Fig. 1 and is in good agreement with measurements of [17].

### 3. CROSS PHASE MODULATION VIA THE QUANTUM WAKE

Following the revivals of molecular alignment, the refractive index of the molecular gas along the pump polarization is periodically modulated and can be expressed as  $\delta n(r, t) = 0.5(\rho_0 \Delta \alpha / n_0)(\langle \cos^2 \theta \rangle - 1/3) + \delta n_{rR}$  [13], where  $\rho_0$  is the initial molecular density and  $n_0$  is the linear refractive index. The rotational Raman contribution  $\delta n_{rR}$  of the pre-excited molecules describes the molecular contribution to the optical Kerr effect that is modeled as in [17] and effectively depends on the pump intensity. Depending whether the molecules are oriented parallel or perpendicular to the field polarization, the refractive index is correspondingly increased or decreased, as presented in Fig. 2.

The revivals of molecular alignment therefore induce an additional nonlinear phase shift  $\varphi_m$  to a properly matched ultrashort probe pulse corresponding to a spectral phase modulation given by  $\delta \omega(t) = -\partial \varphi_m / \partial t \sim -\partial \delta n(t) / \partial t$  [18]. In addition, the transverse profile of the pump pulse remains approximately Gaussian along propagation, i.e., more intense in the central part, leading to a larger degree of molecular alignment in the beam center than in its periphery. Correspondingly, a probe pulse properly matching the

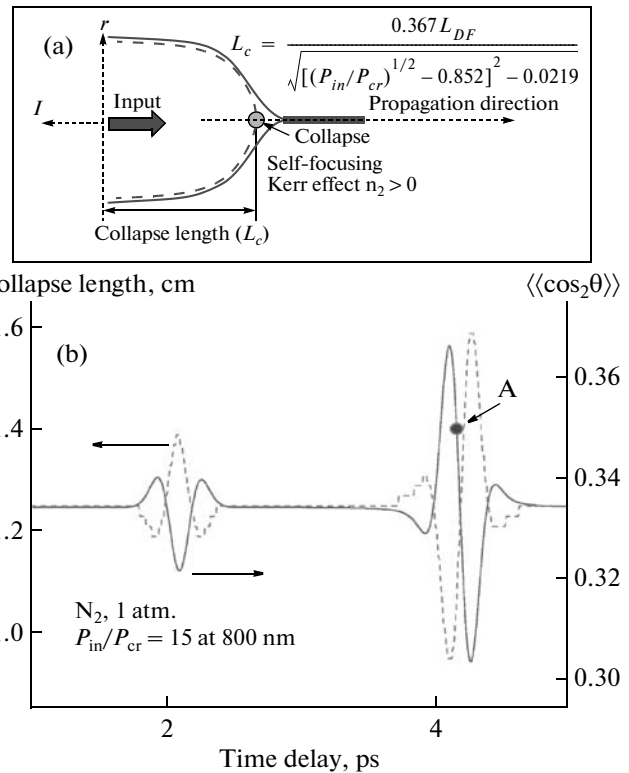


**Fig. 3.** (a) Schematic representation of self-focusing of a Gaussian beam in a Kerr medium and its subsequent collapse. (b) The modulation of the collapse length (dashed curve) follows the revivals

parallel or perpendicular orientation of the molecules during the revival will experience an additional cross-focusing or defocusing effect, respectively. This effect allows us to control the onset of filamentation since the collapse length, defined as the propagation distance to the nonlinear focus of the probe beam and well reproduced by the Marburger law for randomly oriented molecules (see Fig. 3a), can be decreased when the pre-aligned molecules are parallel to the probe polarization or increased in the case of perpendicular alignment (see Fig. 3b) [13].

Therefore, as schematically presented in Fig. 2, the space- and time-dependent quantum revival of molecular alignment acts as a XPM effect on a properly matched probe pulse, thereby opening possibilities to control both its spectral and spatial filamentation dynamics.

Figure 4 shows the typical experimental setup used in our studies for filamentation control. A femtosecond pulse at 800 nm delivered by a 1 kHz Ti:sapphire amplified laser system was first split into a pump used for molecular alignment and a probe pulse used for investigating its propagation dynamics. The pulses were then re-combined and collinearly focused with a lens into a gas cell. The relative delay between pump and probe pulses was controlled by using a motorized translation stage in the pump arm. The polarization of

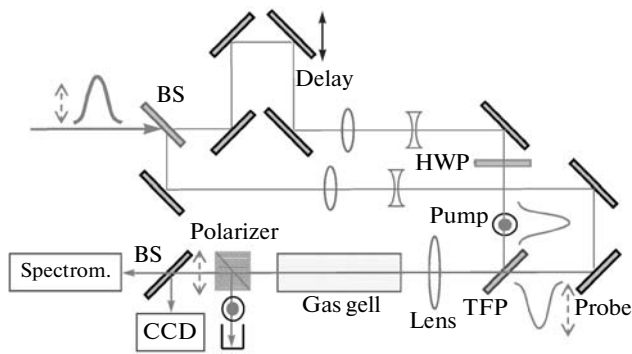


**Fig. 4.** The typical experimental setup used in our studies on filamentation control by molecular alignment. BS: beam splitter, HWP: half-wave plate, TFP: thin film polarizer, CCD: charge coupled device.

the pump pulse was rotated to be orthogonal to the probe by using a half-wave plate in the pump arm just before the re-combination mirror. At the exit of the gas cell, the spectral and spatial profiles of the probe pulse were measured simultaneously by using a spectrometer and a CCD camera after a polarization analysis (polarizer), which reflected the s-polarized pump and transmitted the p-polarized probe. This setup was used for different experiments discussed below, with lenses of different focal lengths, input laser pulses of different energies and durations, and gas cells filled with various molecular gases ( $N_2$ ,  $O_2$ , or  $CO_2$ ) at different gas pressures.

Figure 5a shows the calculated time-dependent spectral modulation (dashed curve) expected from the revival of molecular alignment (solid curve). It suggests that new redder or bluer frequencies should appear when the temporal peak of the probe pulse is tuned to the rising or falling edge of the revival, respectively [13, 18]. The measured spectral modulation of a femtosecond laser pulse propagating in pre-aligned molecular  $N_2$  is shown in Figs. 5b and 5c for two delays corresponding to the rising and falling edge of the revival, as indicated in Fig. 5a. Here, the orthogonally polarized pump (0.7 mJ) and probe pulses (0.2 mJ) with a temporal duration of 50 fs were collinearly focused with a lens of  $f = 40$  cm into a gas cell filled with pure  $N_2$  gas at a pressure of 2 atm. As expected [18], owing to the nonlinear phase shift induced by the revival of molecular alignment, the spectrum of the probe pulse was red-shifted for delay-A (Fig. 5b) or blue-shifted (Fig. 5c) for delay-C matching the rising or falling edges of the quantum revivals, respectively. Due to the additional cross-(de)focusing effect and its spectral counterpart, namely self-phase modulation (SPM), the spectrum of the probe pulse was correspondingly broadened for molecular alignment revival with transient orientation parallel to the field polarization, or narrowed in the case of perpendicular orientation.

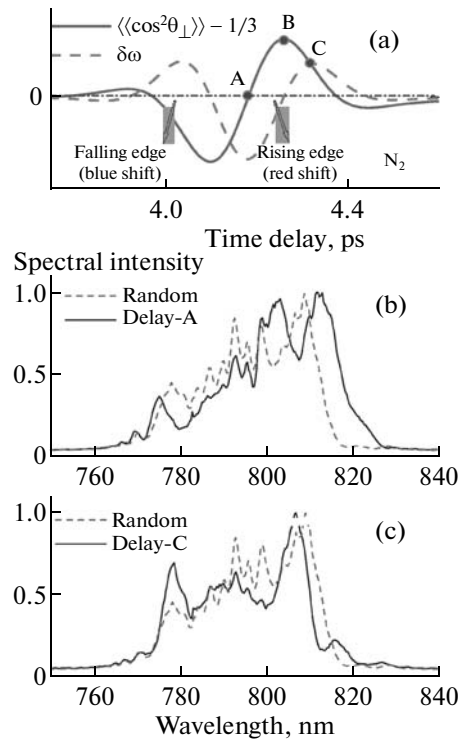


**Fig. 5.** (a) The spectral modulation (dashed curve) induced by the revivals of molecular alignment (solid curve) for  $N_2$ , where  $\theta_{\perp}$  is the angle between the molecular axis and the probe polarization. The measured spectral modulation of the 50 fs probe pulse when its temporal peak is tuned to match the molecular alignment revivals at (b) delay-A and (c) delay-C as labeled in Fig. 5a [18].

The cross-(de)focusing effect was further analyzed by considering a small part of the probe beam which exhibits a modulation of its energy content following the periodic revivals of the molecular alignment. For instance, as shown in Fig. 6a, the center of the probe beam was selected by an aperture of diameter  $D$  (much smaller than the beam waist), leading to a measured signal inversely proportional to  $1 - \eta(\langle\langle\cos^2\theta\rangle\rangle - 1/3)^2$ , where  $\eta$  is a scaling factor linked to the polarizability difference  $\Delta\alpha$ , the gas density, the interaction distance of the molecular gas as well as the aperture diameter. The molecular alignment signal is thus expected to relatively increase for the parallel orientation transient ( $\langle\langle\cos^2\theta\rangle\rangle - 1/3 > 0$ ) and decrease in the perpendicular case ( $\langle\langle\cos^2\theta\rangle\rangle - 1/3 < 0$ ). Experimentally, our cross-(de)focusing assisted polarization spectroscopy for measuring molecular alignment is similar to the conventional polarization spectroscopy technique [16] but only a small part at the beam center of the probe pulse is collected (see Fig. 6a) and analyzed after an  $\alpha$ -BBO polarizer.

Figures 6b–6d show the signals corresponding to revivals of molecular alignment for  $N_2$  measured at various pump intensities by means of our cross-(de)focusing assisted polarization spectroscopy. The

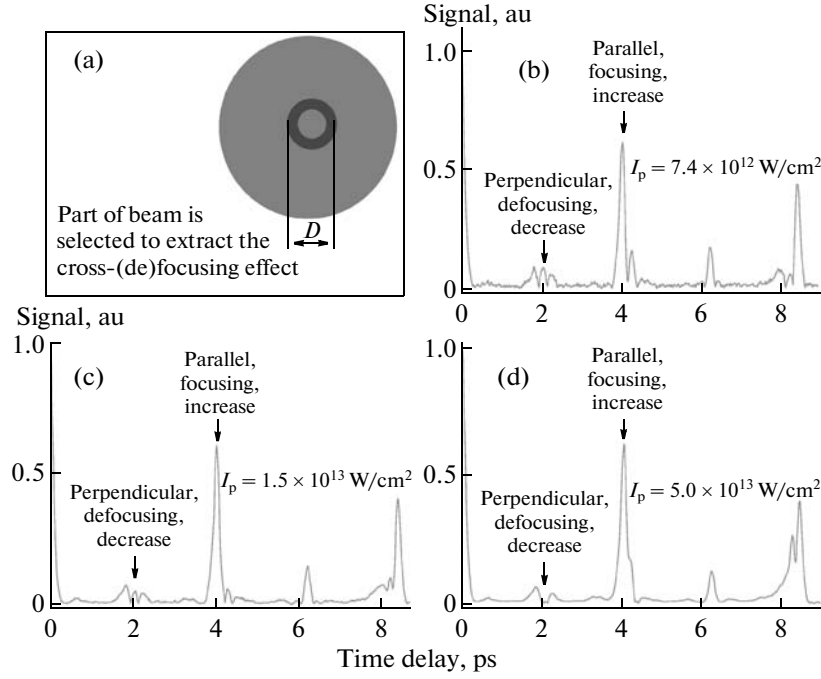


**Fig. 6.** (a) Analysis of the cross-(de)focusing effect by selecting a small part at the center of the probe beam. (b–d) Signals corresponding to revivals of molecular alignment for  $\text{N}_2$  measured at various pump intensities by means of cross-(de)focusing assisted polarization spectroscopy.

molecular alignment signal increases or decreases as expected for parallel and perpendicular transient orientations when the pump intensity increases. In addition, owing to the double-well potential structure of the diatomic molecules, the parallel orientated molecule shows a much higher ionization probability than the perpendicular one [19, 20]. This leads to an anisotropic depletion of neutral molecules with different orientations and hence to a modulation of the refractive index difference which reads  $\Delta n = n_{\parallel} - n_{\perp} \sim BW/3 + (3 - 3AW + BW)(\langle \cos^2\theta \rangle - 1/3)$ , where  $W$  is the ionization rate for randomly orientated molecules, and  $A$  and  $B$  are the parameters used to characterize the orientation-dependent ionization probability and can be derived from [11]. For high pump intensities with noticeable ionization probabilities, this effect also contributes to the measured molecular alignment signal as the cross-(de)focusing effect does, which yields an enhancement of the signal by  $\sim 3\%$  at a pump intensity of  $5.0 \times 10^{13} \text{ W/cm}^2$  as shown in Fig. 6d. Therefore, our hybrid technique for the measurement of molecular alignment can be used not only to identify the transient orientation of the molecules based on the asymmetric evolution of the signal profiles, but also to study the weak ionization dynamics associated with the impulsive rotational Raman excitation. Regarding the filamentation dynamics in molecular gases (e.g., air), the method can be used to characterize ionization as well as the clamping intensity inside the intense core [1, 2].

## 5. CONTROL OF THE FILAMENT LENGTH AND SHOCK-X WAVE GENERATION

By including the contribution of the revivals of molecular alignment to the refractive index, the propagation of an ultrashort laser pulse in pre-aligned molecules can be modeled as [13]:

$$\begin{aligned} \frac{\partial E}{\partial z} = & \frac{i}{2k_0} U^{-1} \left( \frac{\partial^2}{\partial r^2} + \frac{1}{r} \frac{\partial}{\partial r} \right) E - i \frac{k_0^{(2)}}{2} \frac{\partial^2 E}{\partial t^2} + \frac{k_0^{(3)}}{6} \frac{\partial^3 E}{\partial t^3} \\ & + U^{-1} \left[ T^2 i k_0 (n_2 |E|^2 + \delta n) E - \frac{\sigma}{2} (1 + i \omega_0 \tau_c) \rho E \right. \\ & \left. - T \frac{\beta_K}{2} |E|^{2K-2} \left( 1 - \frac{\rho}{\rho_0} \right) E \right]. \end{aligned} \quad (3)$$

Here,  $k_0$  is the wave-number of the ultrashort laser pulse centered at 800 nm,  $k_0^{(2)}$  and  $k_0^{(3)}$  are the second- and third-order dispersions. The operators  $U$  and  $T$  account for space-time focusing and self-steepening of the ultrashort laser pulse. The cross-section  $\sigma$  stands for inverse Bremsstrahlung,  $\beta_K$  accounts for multiphoton absorption, and  $n_2$  denotes the nonlinear refractive index. The electron density  $\rho$  is calculated by resolving  $\partial \rho / \partial t = \sigma_K |E|^{2K} (\rho_0 - \rho)$  at each propagation step, where  $\sigma_K$  denotes the ionization cross-section which accounts for the dependence upon molecular orientation as  $\sigma_K = \sigma_{K0} [1 + (1.5a_2 - 3.75a_4)(\langle \cos^2\theta \rangle - 1/3) + 4.375a_4(\langle \cos^4\theta \rangle - 1/5)]$

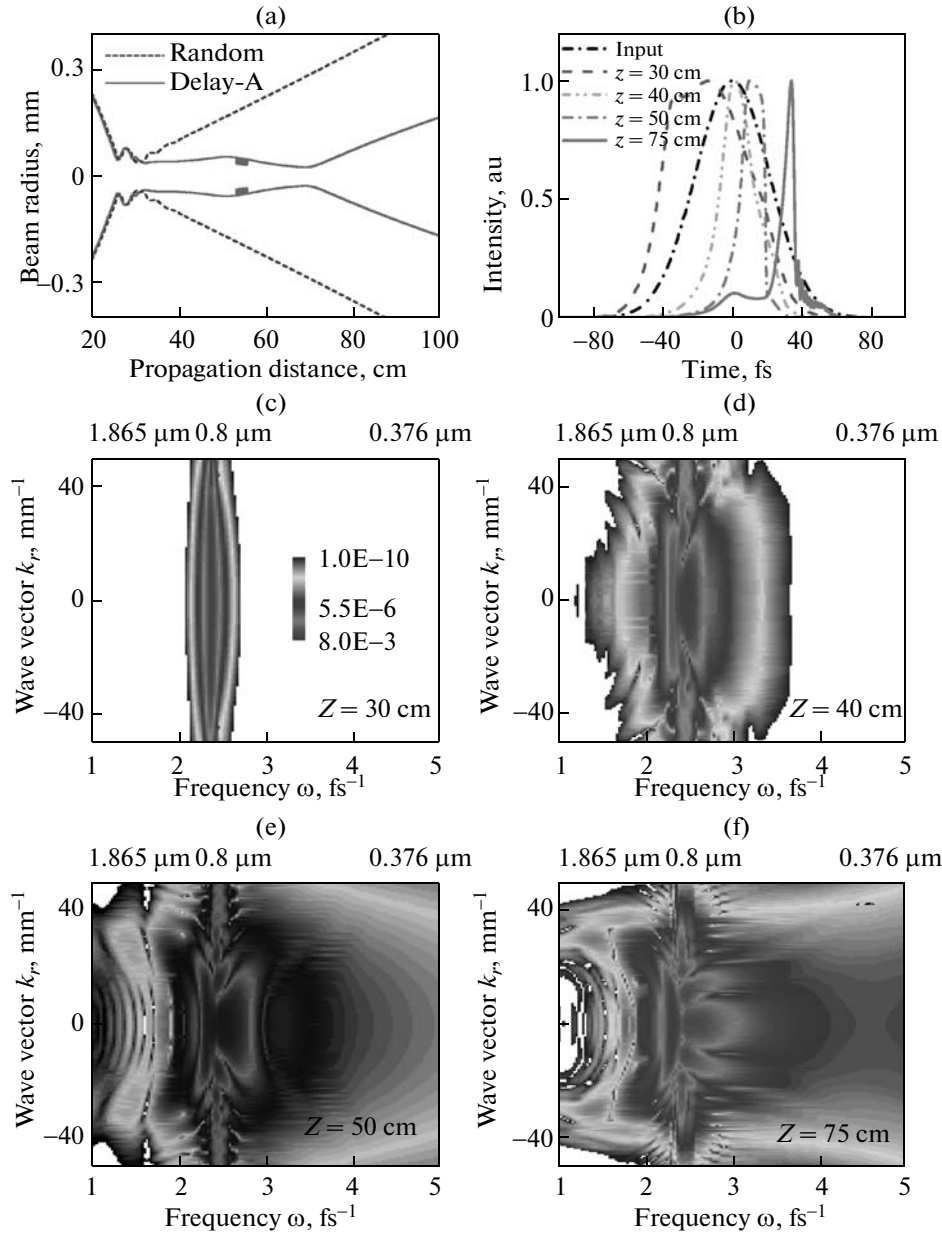


**Fig. 7.** Filamentation and shock X-wave formation in pre-aligned N<sub>2</sub> molecules at a gas pressure of 1 atm. (a) Beam radius of the probe pulse as a function of the propagation distance in the cases of parallel molecular orientation (delay-A as labeled in Fig. 3(b)) and random orientation. On-axis temporal profiles (b) and far-field intensity distributions (c, d, e, f) (log scale) of the probe pulse at propagation distances of 30, 40, 50, and 75 cm.

[11] and  $\sigma_{k0}$  denotes the ionization cross section for randomly aligned molecules. For our simulations, we considered nitrogen at a pressure of 1 atm, which corresponds to the coefficients:  $k_0^{(2)} = 0.2 \text{ fs}^2/\text{cm}$ ,  $k_0^{(3)} = 0.1 \text{ fs}^3/\text{cm}$ ,  $\sigma_{k0} = 6.31 \times 10^{-140} \text{ s}^{-1} \text{ cm}^{22}/\text{W}^{11}$ ,  $a_2 = 0.39$ , and  $a_4 = -0.21$ . The pump and probe pulses are assumed to have the same initial polarization, beam waist, central wavelength and temporal duration, except if otherwise specified. Both the probe and pump pulses were focused by using a lens of focal

length  $f = 30 \text{ cm}$ . The pump pulse used for molecular alignment was set to have a peak intensity of  $2 \times 10^{13} \text{ W}/\text{cm}^2$  at the geometric focus of the lens, thus never leading to significant ionization. Its evolution along the propagation axis therefore obeys the laws of Gaussian optics.

As shown in Fig. 7a, filamentation of the probe pulse reaches  $\sim 50 \text{ cm}$  when the probe matches the revival of molecular alignment at delay-A as labeled in Fig. 3b (polarization parallel to the molecular orientation). This is a considerably longer distance than that

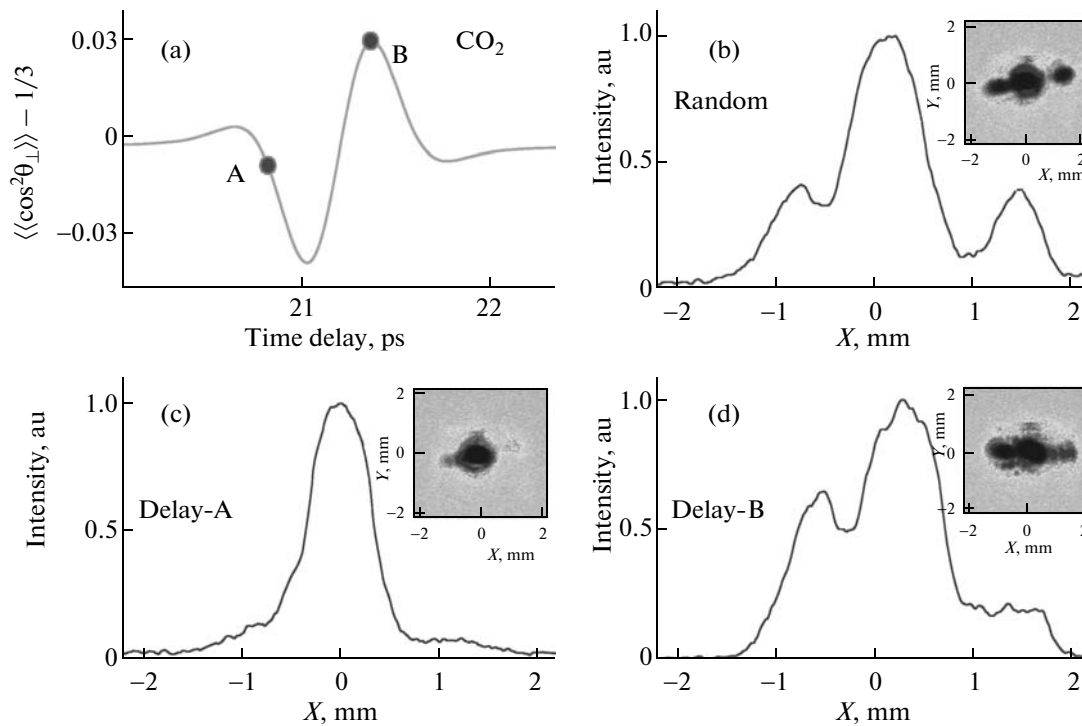


**Fig. 8.** (a) The calculated molecular alignment signal around the half revival time of molecular  $\text{CO}_2$ . The measured spatial profiles of the probe pulse integrated over the  $y$ -axis for (b) randomly oriented molecules (no pump) or (c, d) molecular alignment for which the peak of the probe pulse matches delay-A (c) and delay-B (d) of the revival as labeled in (a). The insets in (b–d) show the filamentation pattern (beam cross section) recorded by using the CCD camera.

reached in the case of randomly oriented  $\text{N}_2$  molecules (dashed curve). The temporal duration, beam diameter, and peak power of the input probe pulse were 50 fs, 1.5 mm, and  $2P_{\text{cr}}$ , respectively, where  $P_{\text{cr}} = 4.4$  GW is the critical power for self-focusing in  $\text{N}_2$  (at 1 atm and 800 nm). Filamentation is associated with significant spatiotemporal reshaping of the pulse leading to a self-shortening effect [5, 21]. Molecular alignment with a pump pulse allows for a control of the self-shortening of a delayed probe pulse undergoing filamentation [13]. As shown in Fig. 7b, the probe pulse with an input temporal duration of 50 fs was dramatically compressed down to 5.6 fs with a falling edge featured by an optical shock associated with a significant spectral blue-shift [22, 23].

It was demonstrated that filamentation of ultrashort laser pulses leads to the spontaneous formation of nonlinear conical waves which are stationary non-diffractive and non-dispersive wave-packets supported by a conical energy flux from the periphery toward the intense central part of the wave [24]. These peculiar wave-packets not only exhibit a conical shape in the near-field, as shown by measurements based on a 3D mapping technique [25], but also in the far-field ( $\theta, \lambda$ ) or equivalently ( $k_r, \omega$ ) and were therefore called X-waves [26]. The X shaped structure of the far-field reflects the fact that conical emission with different frequencies propagating at different angles is gener-

ated from the filament and measurements can be fully interpreted from the knowledge of the dispersive properties of the medium [24]. In addition, conical emission and axial supercontinuum were interpreted as parts of the same physical process identified as the formation of a shock-X wave [23]. Here, we show that the quantum revival of molecular alignment can act as a control mechanism for the formation of shock-X-waves [13]. Figs. 7c–7f show that at delay-A (as labeled in Fig. 3b), an X-shaped angular spectrum featured by an on-axis blue-shifted super continuum and red-shifted conical tails is gradually generated along the propagation axis, in spite of our moderate input power. This far-field corresponds to the few-cycle pulse with a falling shock edge shown in Fig. 7b (red-solid curve). The red-shifted conical tails result from the excitation of the redder frequency components in the leading part of the probe pulse, and their subsequent diffraction while they travel faster than the initial group velocity  $v_g(\omega_0)$  of the wave-packet to reach the region of weak intensities ahead the peak of the pulse. For the case of randomly oriented molecules without pump pulse, the probe pulse with the same input duration and power propagates without forming any X-shaped wave. Molecular pre-alignment therefore constitutes a simple and unique method to promote the spontaneous generation of shock X-waves in a filament and tune their characteristics [13].

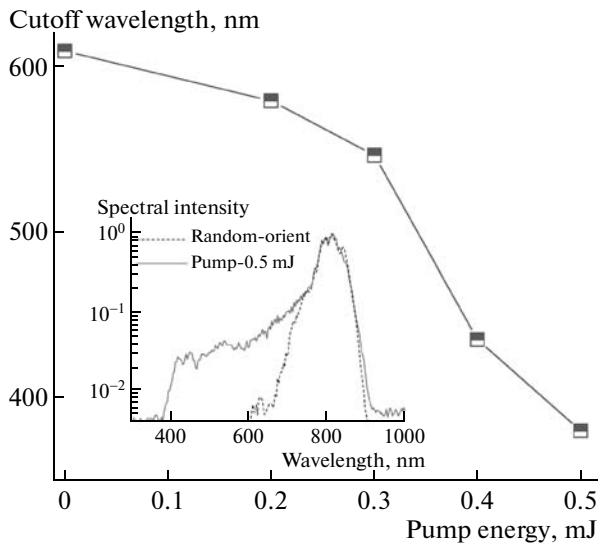


**Fig. 9.** Cutoff wavelength of the probe pulse in the ultraviolet spectral region for different pump intensities. The probe was tuned to match the revival of molecular alignment at delay-B as labeled in Fig. 8a. The inset shows a comparison of the measured spectra of the probe pulse for a pump energy of 0.5 mJ and for a random orientation of the molecules.

## 6. CONTROL OF MULTIPLE FILAMENTATION

Instead of a single filament, multiple filamentation typically occurs when an intense ultrashort laser pulse propagates in a transparent nonlinear medium in the presence of symmetry breaking effects such as noise, vectorial effects, turbulence, etc. [27–29]. Multiple filamentation patterns were demonstrated to be controllable by adjusting intensity or phase gradients, astigmatism [30] or ellipticity [31] of the incident beam. We found that the multiple filamentation dynamics of the probe pulse could be controlled by using the spatiotemporal coupling induced by XPM originated from the revivals of molecular alignment. In our experiments, after a thin film polarizer for beam recombination, the collinear *s*-polarized pump pulse ( $\sim 0.6$  mJ) for molecular alignment and *p*-polarized probe pulse ( $\sim 1.05$  mJ) for filamentation were both focused (focal length  $f = 50$  cm) into a 60 cm gas cell filled with pure molecular  $\text{CO}_2$  at a pressure of 2 atm. The spatial and spectral profiles of the probe pulses were then analyzed simultaneously by a CCD and a spectrometer after an  $\alpha$ -BBO polarizer (see Fig. 4).

Without pump, the probe pulse with an input spatial ellipticity of  $e \sim 1.5$  forms three hot spots aligned along the long axis of the beam profile (see Fig. 8b; a similar effect was reported in [32]). As shown in Fig. 8c, by switching on the pump and tuning the peak of the probe to match delay-A (labeled in Fig. 8a) on the negative side of the revival of molecular, the three hot spots are suppressed; a single filament is thus obtained in perpendicularly oriented molecules due to

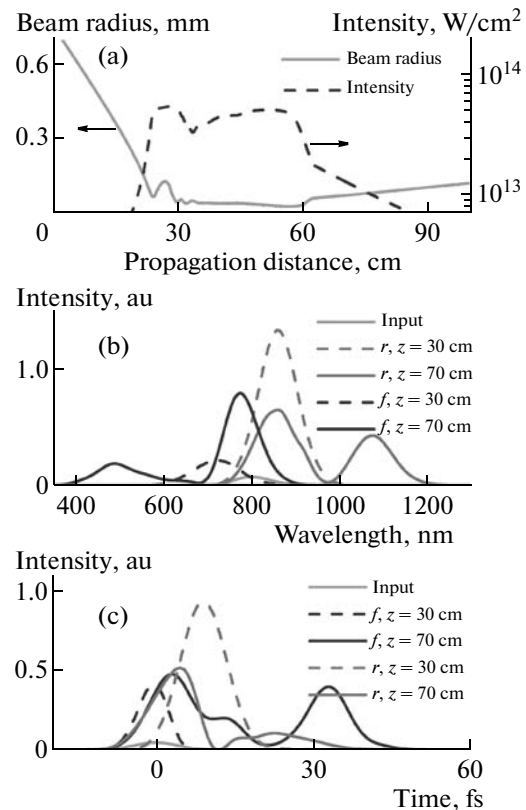


**Fig. 10.** Frequency tuning of a few cycle probe pulse by means of filamentation and molecular alignment of an intense pump pulse. (a) The beam radius (solid curve) and peak intensity (dashed curve) of the pump pulse as it propagates in randomly oriented molecular  $\text{N}_2$ . The spectra (b) and temporal profiles (c) of the probe pulse at various propagation distance when it is respectively tuned to match the rising- (red curve, labeled as *r*) and falling-edges (blue curve, labeled as *f*) of the revivals of molecular alignment inside the pump filament.

the weakening of SPM leading to a narrower spectrum and a cross-defocusing effect. In contrast, SPM was enhanced on the positive side of the revival and the associated cross-focusing effect originating from the parallel orientation of the molecules leads to the observation of band- or ripple-like beam profiles of the probe pulse with broadened spectra. For example, as shown in Fig. 8d, for delay-B (labeled in Fig. 8a), the probe pulse was regularized to have a ripple-like structure. The multiple filamentation dynamics of the probe pulse could thus be controlled to display various beam patterns with correspondingly modulated spectra by means of the quantum wake of the molecular alignment.

## 7. CONTROL OF SUPERCONTINUUM GENERATION

Supercontinuum generation by self-guided filaments was investigated extensively [7, 8]. Recently, Kolesik et al. have shown from numerical simulations

that XPM between a pump and a closely following probe pulse (several hundred of femtoseconds) allows for an enhancement of the supercontinuum generated by the probe pulse [33]. Here, by using the quantum revivals of the molecular alignment, we show experimentally that supercontinuum generation can also be controlled [13]. The experiments were performed with an amplified femtosecond pulse with duration of 35 fs at 800 nm. Both the pump and probe pulses were focused by a lens of  $f = 60$  cm into a 85 cm-long gas cell, which was filled with pure molecular  $\text{CO}_2$  with a maximum gas pressure of 2 atm. The final pulse energies for the pump and probe pulses before the gas cell were respectively measured to be 0.5 and 1.5 mJ, and the probe pulse energy was slightly higher than that used for multiple filamentation.

As shown in Fig. 9, for parallel orientation transient of the molecular alignment with the maximum value of  $\langle\langle\cos^2\theta\rangle\rangle$  around the half-revival time (delay-B in Fig. 8a), the ultraviolet cutoff wavelength of the probe pulse decreased gradually when the pump intensity was increased. This finally led to a cutoff around 380 nm with a broadband plateau for a pump energy of 0.5 mJ as shown in the inset, whereas the cutoff wavelength obtained with the same probe pulse and a random molecular orientation lies around 600 nm. In addition to the supercontinuum generation, a self-cleaning effect of the probe pulse was also observed, as reported in [34]. The incident beam with an input spatial ellipticity of  $e \sim 1.6$  led to multiple filaments along the long axis of the incident beam in randomly oriented molecules, whereas a self-cleaned single beam profile was obtained with preliminary alignment of the molecules with the 0.5 mJ pump. We attribute this effect to an indirect effect of supercontinuum generation, which redistributed the available energy over a broad spectral range and thus decreased the peak intensity around the central wavelengths of the incident probe. This suppressed the beam breakup and led to the observed single core beam. A similar control of supercontinuum generation was also observed in diatomic molecules of  $\text{N}_2$  and  $\text{O}_2$  [13]. A more significant dependence on the degree of molecular alignment was observed for molecular  $\text{O}_2$  owing to its larger polarizability difference with respect to molecular  $\text{N}_2$ .

## 8. TUNING OF FEW-CYCLE LASER PULSE

Tuning few-cycle laser pulses to wavelengths different from the fundamental and its harmonics is very important for various applications. This was demonstrated to be achievable by using conventional non-collinear optical parametric amplifications (NOPAs) in a thin nonlinear crystal [35, 36], four-wave mixing (FWM) processes in filaments [37], or molecular phase modulation in hollow fibers [38–40]. We show here that tuning of few-cycle laser pulses can also be achieved by using filament propagation and the quan-

tum revivals of molecular alignment [13]. In contrast with previous studies, the pump is now sufficiently intense to form a filament with a stable high intensity and a well confined beam diameter over a propagation distance much longer than the Rayleigh range. This provides us with a steady channel to manipulate the molecular orientation and thus to induce a continuous frequency shift on a properly delayed few-cycle laser pulse.

We performed a numerical experiment in molecular  $\text{N}_2$  at a gas pressure of 1 atm. As shown in Fig. 10a, a self-guided filament with a stable peak intensity of  $\sim 5.0 \times 10^{13}$  W/cm<sup>2</sup> and beam radius of  $\sim 50$   $\mu\text{m}$  over a propagation distance of  $\sim 38$  cm is obtained by focusing (focal length  $f = 30$  cm) a 50 fs pump pulse with input power and beam diameter of  $P_{\text{in}} = 2.0P_{\text{cr}}$  and 1.5 mm. Figure 10b shows that the spectrum of a few-cycle probe pulse of 10 fs was respectively red- or blue-shifted when the peak of the probe matches the rising (labeled as  $r$ ) or falling (labeled as  $f$ ) edge of the molecular alignment revival inside the pump filament (Fig. 10a). Interestingly, the central wavelength of the few-cycle probe could be up-shifted or down shifted by several hundreds of nm. The pulse duration of the probe remained close to the input value of 10 fs as shown in Fig. 10c. Therefore, in addition to the conventional NOPAs and FWM processes [35–37], the rotational Raman effect in the wake of femtosecond filament provides us a flexible approach to tune the frequency of few-cycle laser pulses.

## 9. CONCLUSIONS

In summary, the filamentation dynamics of a femtosecond laser pulse can be readily controlled by means of the quantum wake of a pump pulse, generally used for molecular alignment. By properly delaying a probe pulse, we controlled the XPM effect induced via the field-free revivals of the molecular alignment. The filamentation dynamics of the probe pulse then becomes no longer spontaneous but strongly depends on the part of the revival experienced by the probe. Several features of the filament can be directly or indirectly controlled. Beyond the observations discussed here, including the filamentation length, multiple filamentation dynamics, shock X-wave generation, supercontinuum emission, and wavelength tuning of few-cycle laser pulses, the quantum-wake based control can be applied for atmospheric applications and remote probing of aerosols with intense femtosecond filaments.

## ACKNOWLEDGMENTS

This work was funded in part by National Natural Science Fund (Grants 10525416 and 10804032), National Key Project for Basic Research (Grant 2006CB806005), Project from Shanghai Science and Technology Commission (Grant 08ZR1407100), Pro-

gram for Changjiang Scholars and Innovative Research Team in University, and Shanghai Educational Development Foundation (Grant 2008CG29).

## REFERENCES

1. S. L. Chin, S. A. Hosseini, W. Liu, Q. Luo, F. Théberge, N. Aközbek, A. Becker, V. P. Kandidov, O. G. Kosareva, and H. Schroeder, *Can. J. Phys.* **83**, 863 (2005).
2. A. Couairon and A. Mysyrowicz, *Phys. Rep.* **441**, 47 (2007).
3. G. Méan, J. Kasparian, E. Salmon, J. Yu, J.-P. Wolf, R. Bourayou, R. Sauerbrey, M. Rodriguez, L. Wöste, H. Lehmann, B. Stecklum, U. Laux, J. Eislöffel, A. Scholz, and A. Hatzes, *Appl. Phys. B* **77**, 357 (2003).
4. C. P. Hauri, W. Kornelis, F. W. Helbing, A. Heinrich, A. Couairon, A. Mysyrowicz, J. Biegert, and U. Keller, *Appl. Phys. B* **79**, 673 (2004).
5. A. Couairon, J. Biegert, C. P. Hauri, W. Kornelis, F. W. Helbing, U. Keller, and A. Mysyrowicz, *J. Mod. Opt.* **53**, 75 (2006).
6. S. Chin, F. Théberge, and W. Liu, *Appl. Phys. B* **86**, 477 (2007); H. S. Chakraborty, M. B. Gaarde, and A. Couairon, *Opt. Lett.* **31**, 3662 (2006); A. Couairon, H. S. Chakraborty, and M. B. Gaarde, *Phys. Rev. A* **77**, 053814 (2008).
7. J. Kasparian, R. Sauerbrey, D. Mondelain, S. Niedermeyer, J. Yu, J.-P. Wolf, Y. André, M. Franco, B. Prade, S. Tzortzakis, A. Mysyrowicz, M. Rodriguez, H. Wille, and L. Wöste, *Opt. Lett.* **25**, 1397 (2000).
8. F. Théberge, W. Liu, Q. Luo, and S. L. Chin, *Appl. Phys. B* **80**, 221 (2005).
9. C. D'Amico, A. Houard, S. Akturk, Y. Liu, J. Bloas, M. Franco, B. Prade, A. Couairon, V. T. Tikhonchuk, and A. Mysyrowicz, *New J. Phys.* **10**, 013015 (2008).
10. J. Itatani, J. Levesque, D. Zeidler, H. Niikura, H. Pépin, J. Kieffer, P. Corkum, and D. Villeneuve, *Nature* **432**, 867 (2004).
11. T. Kanai, S. Minemoto, and H. Sakai, *Nature* **435**, 470 (2005); J. Wu, H. Qi, and H. Zeng, *Phys. Rev. A* **77**, 053412 (2008).
12. F. Calegari, C. Vozzi, S. Gasilov, E. Benedetti, G. Sansone, M. Nisoli, S. De Silvestri, and S. Stagira, *Phys. Rev. Lett.* **100**, 123006 (2008).
13. J. Wu, H. Cai, H. Zeng, and A. Couairon, *Opt. Lett.* **33**, 2593 (2008); J. Wu, H. Cai, A. Couairon, and H. Zeng, *Phys. Rev. A* **79**, 063812 (2009); J. Wu, H. Cai, Y. Peng, and H. Zeng, *Phys. Rev.* **79**, 041404(R) (2009); H. Cai, J. Wu, Y. Peng, and H. Zeng, *Opt. Express* **17**, 5822 (2009); J. Wu, H. Cai, A. Couairon, and H. Zeng, *Phys. Rev. A* (2009), in press.
14. S. Varma, Y.-H. Chen, and H. M. Milchberg, *Phys. Rev. Lett.* **101**, 205001 (2008).
15. H. Stapelfeldt and T. Seideman, *Rev. Mod. Phys.* **75**, 543 (2003).
16. V. Renard, M. Renard, S. Guérin, Y. T. Pashayan, B. Lavorel, O. Faucher, and H. R. Jauslin, *Phys. Rev. Lett.* **90**, 153601 (2003).
17. E. Nibbering, G. Grillon, M. Franco, B. Prade, and A. Mysyrowicz, *J. Opt. Soc. Am. B* **14**, 650 (1997).
18. H. Cai, J. Wu, A. Couairon, and H. Zeng, *Opt. Lett.* **34**, 827 (2009).
19. I. Litvinyuk, K. Lee, P. Dooley, D. Rayner, D. Villeeneuve, and P. Corkum, *Phys. Rev. Lett.* **90**, 233003 (2003).
20. J. Wu, H. Zeng, and C. Guo, *Phys. Rev. A* **75**, 043402 (2007); J. Wu, H. Zeng, and C. Guo, *J. Phys. B* **40**, 1095 (2007).
21. A. Mysyrowicz, A. Couairon, and U. Keller, *New J. Phys.* **10**, 025023 (2008); S. Akturk, A. Couairon, M. Franco, and A. Mysyrowicz, *Opt. Express* **16**, 17626 (2008).
22. A. Gaeta, *Phys. Rev. Lett.* **84**, 3582 (2000).
23. F. Bragheri, D. Faccio, A. Couairon, A. Matijosius, G. Tamošauskas, A. Varanavicius, V. Degiorgio, A. Piskarskas, and P. Di Trapani, *Phys. Rev. A* **76**, 025801 (2007).
24. D. Faccio, A. Averchi, A. Lotti, P. Trapani, A. Couairon, D. Papazoglou, and S. Tzortzakis, *Opt. Express* **16**, 1565 (2008); D. Faccio, M. A. Porras, A. Dubietis, G. Tamosaukas, E. Kucinskas, A. Couairon, and P. Di Trapani, *Opt. Commun.* **265**, 672 (2006).
25. D. Faccio, A. Matijosius, A. Dubietis, R. Piskarskas, A. Varanavicius, E. Gaizauskas, A. Piskarskas, A. Couairon, and P. Trapani, *Phys. Rev. E* **72**, 037601 (2005).
26. W. Lei, J. Wu, H. Cai, and H. Zeng, *Opt. Lett.* **34**, 166 (2009).
27. M. Mlejnek, M. Kolesik, J. V. Moloney, and E. M. Wright, *Phys. Rev. Lett.* **83**, 2938 (1999).
28. G. Fibich and B. Ilan, *Opt. Lett.* **26**, 840 (2001).
29. A. Houard, M. Franco, B. Prade, A. Durécu, L. Lombard, P. Bourdon, O. Vasseur, B. Fleury, C. Robert, V. Michau, A. Couairon, and A. Mysyrowicz, *Phys. Rev. A* **78**, 033804 (2008).
30. G. Méchain, A. Couairon, M. Franco, B. Prade, and A. Mysyrowicz, *Phys. Rev. Lett.* **93**, 035003 (2004).
31. T. Grow and A. Gaeta, *Opt. Express* **13**, 4594 (2005).
32. A. Dubietis, G. Tamosauskas, G. Fibich, and B. Ilan, *Opt. Lett.* **29**, 1126 (2004).
33. M. Kolesik, D. E. Roskey, and J. V. Moloney, *Opt. Lett.* **32**, 2753 (2007).
34. B. Prade, M. Franco, A. Mysyrowicz, A. Couairon, H. Buersing, B. Eberle, M. Krenz, D. Seiffer, and O. Vasseur, *Opt. Lett.* **31**, 2601 (2006).
35. G. Cerullo, M. Nisoli, S. Stagira, S. De Silvestri, G. Tempea, F. Krausz, and K. Ferencz, *Opt. Lett.* **24**, 1529 (1999).
36. A. Shirakawa, I. Sakane, M. Takasaka, and T. Kobayashi, *Appl. Phys. Lett.* **74**, 2268 (1999).
37. F. Théberge, N. Aközbek, W. Liu, A. Becker, and S. L. Chin, *Phys. Rev. Lett.* **97**, 023904 (2006).
38. R. Bartels, T. Weinacht, N. Wagner, M. Baertschy, C. Greene, M. Murnane, and H. Kapteyn, *Phys. Rev. Lett.* **88**, 013903 (2001).
39. N. Zhavoronkov and G. Korn, *Phys. Rev. Lett.* **88**, 203901 (2002).
40. F. Zhong, H. Jiang, and Q. Gong, *Opt. Express* **17**, 1472 (2009).